Available online at www.sciencedirect.com
SCIENCE DIRECT
Journal of Photochemistry and Photobiology A: Chemistry 174 (2005) 62–70
Journal of Photochemistry and Photobiology A:Chemistry
www.elsevier.com/locate/jphotochem

Fluorescence development during 514 nm irradiation of catechol adsorbed on nanocyrstalline titanium dioxide

D.V. Heyd*, B. Au

Department of Chemistry and Biology, Ryerson University, 350 Victoria Street, Toronto, Ont., Canada M5B 2K3

Received 19 October 2004; received in revised form 2 March 2005; accepted 7 March 2005
Available online 25 April 2005

Abstract

Irradiation of a catechol/TiO_2 film with a 514 nm laser produced a fluorescent, surface-adsorbed species. The reaction was slow, taking approximately 20–60 min to reach completion under the conditions of this study. A laser power study indicated that the rate of reaction was approximately proportional to the square-root of the laser power. The kinetics of fluorescence development could be modelled by a simple, first-order rate law for the nitrogen-sparged solution only. When air was bubbled through the solution the initial rate increased, and a transient peak in the fluorescence could be observed for $\theta = 0.49$ (the lowest coverage in this study). The kinetics of the air-sparged system could be reproduced with a model that included both a persistent fluorescent species and a transient species, which converted to a non-fluorescent product in a subsequent, photochemical reaction. Raman spectra of the fully reacted surface did not reveal any new, adsorbed, organic molecule, indicating that the reaction results in the desorption of the organic molecule. It was concluded that fluorescent species was a modification of the titania surface, likely a partially reduced titanium ion.

Keywords: Raman microscopy; Titanium dioxide; Catechol; Fluorescence; Photochemistry

1. Introduction

Photoluminescence of bare TiO_2 has been the subject of many studies [1–4]. Photoemission has been observed in nanocrystals and crystalline thin films that have been irradiated by ultraviolet light with energy above the band gap. The emission is normally weak, so studies are often conducted at low temperature to reduce non-radiative relaxation processes [1,3]. The broad emission spans much of the visible spectral region (e.g. 430 to >650 nm [1], 470 to >650 nm [3]) and centred in the green (e.g. the centre of the anatase emission has been reported as 500 nm [2], 554 nm [1], and 580 nm [3]). The emission has been ascribed to recombination of electrons and holes at electron trap sites on the surface. The trap sites are thought to be co-ordinatively unsaturated Ti(IV) ions, with energies about 0.3 eV below the conduction band edge [5]. In support of that, an increase in the photoluminescence has been demonstrated for surface treatments (e.g. milling) that generate those trap sites [3]. Adsorption of catechol, benzoate, terephthalate, and isophthalate, which bind trap sites strongly and push their energy levels above the CB band edge, greatly diminishes carrier recombination [5]. One study [6] of dye-sensitised TiO_2 indicated that the energy levels of the trap sites, and hence carrier recombination dynamics, can be manipulated by application of an external bias and by electrolyte composition. A study of anatase films grown by CVD and annealed in O_2 revealed three emission bands centred at 636, 577, and 517 nm. The bands were ascribed to recombination events at O vacancies, relaxation of self-trapped excitons, and recombination at Ti^{3+} sites, respectively [4].

The fluorescence reported in this paper is produced by irradiation of catechol adsorbed on titanium dioxide with 514 nm light. The photon energy is well below the bandgap of titanium dioxide (2.4 eV compared to 3.2 eV), indicating that the well-known charge-transfer complex is the absorb-

* Corresponding author. Tel.: +1 416 979 5000x6553; fax: +1 416 979 5044.
E-mail address: dheyd@ryerson.ca (D.V. Heyd).

1010-6030/$ – see front matter © 2005 Elsevier B.V. All rights reserved.
doi:10.1016/j.jphotochem.2005.03.009

ing species. The fluorescent centres, which are the product of the photoreaction, are also excited by 514 nm light. The photoreaction occurs in nitrogen-purged solutions, as well as oxygen-containing solutions, but the initial rate of reaction is lower in the absence of oxygen. The presence of oxygen results in the destruction of a significant proportion of the fluorescent centres at longer reaction times, so that the ultimate fluorescence intensity is lower in the presence of oxygen. The model proposed for the reaction implies two classes of adsorbed catechol. Those adsorbed in high-free energy sites (defects) can be converted into fluorescent centres, with a subsequent, oxygen-dependent photoreaction that converts them to a non-fluorescent species (transient fluorescent species). Those adsorbed at low-free energy sites can be converted to fluorescent centres, but further reaction to the non-fluorescent species is very difficult, even in the presence of oxygen (persistent fluorescent species).

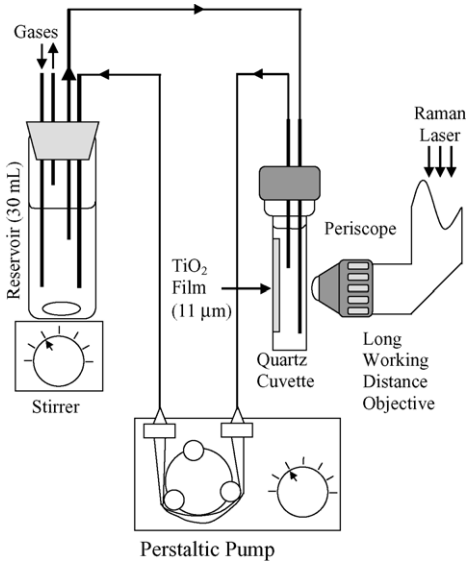

Fig. 1. Experimental apparatus.

2. Experimental

2.1. Raman/fluorescence experiments

All solutions were un-buffered and made from Milli-Q water (>18 MΩ). The titania used in the films was Degussa P25 (70:30 anatase:rutile). Catechol (Aldrich, 99%) solutions were prepared under low-light conditions and wrapped in aluminium foil, to protect them from light. Fresh catechol solutions were prepared for each experiment.

The titania films (Degussa P25) were prepared by pipetting 25 μL of a 52 g L^{-1} slurry onto one of the windows of a 0.5 cm fused-silica cuvette. The area of the window covered by a film was approximately 0.6 cm × 1.6 cm. The film was heated overnight at 200 °C to fix the titania to the window. Assuming a 70:30 mixture of anatase (3.84 g cm^{-3}) and rutile (4.26 g cm^{-3}), and a particle volume fraction of 0.30 [7], film thickness was estimated at 11 μm. Thin films were used to ensure fast mass transport. The films were robust, and lasted several hours under water without noticeable flaking.

A diagram of the apparatus for the photochemistry experiments is shown in Fig. 1. The system used a closed-loop flow cell, fashioned from a screw-top, fused silica fluorescence cell (Spectrocell Inc.), with a path length of 0.5 cm. The long-working distance objectives used in this study required a cell with a short path length. The cell was capped with a PTFE-coated septum, through which the liquid transfer lines ran. The liquid was pumped from a reservoir to the cell, and back again, by a peristaltic pump. The pumping speed was 8 mL min^{-1}, and the total volume was 30 mL, so 3.75 min was required to pump the entire volume once around the cell. Mixing occurred in the reservoir by magnetic stirring. The reservoir was also the site of introduction of catechol and gases (air, O_2, or N_2). The gases were all of pre-purified quality (99.998%) or better, and were bubbled continuously through the solutions in order to keep them saturated.

The surface of the titania was probed by the Raman microscope (Renishaw System 2000) using a periscope with a long-working distance objective (50×). The effective laser-spot size for 514 nm under these conditions was approximately 5 μm. The Raman analyser is a spectrograph design that uses a holographic notch filter to reject the laser line, followed by a diffraction grating to separate the Raman-shifted wavelengths. The wavelengths are then projected onto a CCD detector to obtain a spectrum with 2.5 cm^{-1} resolution. The microscope can also be used to obtain a Raman image of the surface at a particular Raman shift. That is done by irradiating a large area of the surface with a defocused laser beam, filtering the Raman-scattered light through an interference filter (band pass ±20 cm^{-1}), and projecting the image onto the CCD camera.

The 514 nm laser used to probe the surface was also the source of irradiation that induced the photochemical reaction. The "photochemistry" phase of the experiment was usually carried out at high power (2.2 mW at the surface). The exception was during the power dependence study, when the photochemistry phase was performed at 2.2, 0.22, and 0.022 mW (100%, 10%, and 1% laser power). Spectra were not collected during the photochemistry phase; the surface was simply irradiated. The "probe" part of the experiment, during which the fluorescence of the product was measured, was always performed at low power (1% = 0.022 mW), in order to minimise the extent of photochemical reaction during collection of spectra.

The time axes for the kinetic plots of the laser-power dependence studies had to be corrected for the time spent under the laser during the probe phase. Corrections were performed assuming both a linear and a square-root dependence of the reaction rate with laser power, and it was found that the difference between the two methods of correction was small. Because the rate appeared to follow a square-root depen-

dence with laser power, the square-root correction was used for consistency with the observed laser dependence.

The excitation source could be switched from 514 to 785 nm when the Raman signals were of more interest than fluorescence. The spectra collected using the 785 nm laser had lower fluorescence than those collected at 514 nm, so the Raman signals were more easily observed.

Because of the roughness of the films, the raw signals (Raman and fluorescence) were variable, and required normalisation. The titanium dioxide peaks between 100 and 700 cm^{-1}) were used for that purpose. The signals reported are the ratios of the raw intensities to the intensities of the titanium dioxide Raman signals.

2.2. Adsorption isotherm measurements

Because of the reactivity and high fluorescence of the adsorbed catechol complex, the adsorption isotherm was measured by ultraviolet spectroscopy. Films were prepared on the inner walls of nominal 12 mL cylindrical, glass vials. A volume, 1.00 mL, of a 52 g L^{-1} TiO_2 slurry was pipetted to each vial, and then heated to dryness in an oven at 100–150 °C while the vials were rolled back and forth on their sides. A much larger mass of titania was needed for these experiments than for the Raman/fluorescence experiments, because measurement of the isotherm required that a significant fraction of the catechol be adsorbed. (Under the conditions of the Raman/fluorescence experiments, there was little change in the catechol concentration on adsorption.) The films were heated to 200 °C to fix them to the walls of the vials, as for the photochemistry experiments. After cooling the vials to room temperature, 12.0 mL of catechol solution (0–5.00 mM) was added to each. A second set of vials with the same concentrations of catechol, but without titania, were also prepared. Both sets of vials were stored in the dark overnight at 24 °C.

Some flaking of the film was evident, but the flakes were large, and they precipitated. There was some concern that free titania in solution would interfere with the spectra, but no absorbance from titania was observed in the UV spectra of the solutions. The flaking was not expected to affect the surface area of the films. The free particles of the film had a surface area of 2.6 m^2 (0.052 g × 50 m^2 g^{-1}), or 2.6 × 10^4 cm^2. After calcining the film, the area was expected to be lower, but probably on the same order. Flaking only increased the exposed area of the particles by ∼cm^2, or ∼0.01% of the total area.

The spectra of the solutions (200–400 nm) were measured after allowing the vials to reach equilibrium. No solution species other than catechol were evident. The peak at 275 nm was used to determine the catechol content of the solution. (Higher concentrations were diluted to keep the absorbance below 2.5.) The difference in absorbance between the solutions with and without catechol was used to determine the equilibrium concentration of the solution and the amount of catechol adsorbed to the titania.

3. Results and discussion

3.1. Adsorption of catechol on titania

The 24 °C adsorption isotherm for catechol is shown in Fig. 2. Beyond 2.0 mM (equilibrium solution concentration) the isotherm curves upwards, indicating multilayer adsorption (not shown in figure). The data from 0 to 1.7 mM were fitted to a Langmuir isotherm. Full coverage ($\theta = 1$) is 79 μmol catechol per gram of titania. Assuming an adsorption site density for the TiO_2 of approximately 2 nm^{-2} [8] and a specific area of 50 m^2 g^{-1} (as specified by the manufacturer) the number of sites per catechol molecule is approximately 2. That is inconsistent with the previously described bidentate form of the complex (one site per molecule) [7]. However, a significant number of the sites available in the powder are not available in the film, which was heated to increase adhesion. Although the film was porous, it would not be expected to have the same surface area of the free particles. Therefore, 2 may be considered an upper limit to the ratio of sites per catechol molecule; the true value might be much lower. The high equilibrium constant for adsorption (9.7 × 10^3 M^{-1}) indicates that the catechol is strongly chemisorbed, as expected. The equilibrium concentrations used in this study—0.10, 0.25, 0.50, and 1.00 mM—correspond to θ = 0.49, 0.71, 0.83, and 0.91, respectively.

The differences between our Raman spectra of aqueous and adsorbed catechol (Fig. 3), collected with the 785-nm probe laser, indicate the significant changes in the molecular structure expected upon chemisorption. Catechol in water (Fig. 3a) exhibits bands characteristic of an *ortho*-disubstituted aromatic compound [9]. The resonance at 1598 cm^{-1} is due to aromatic C=C stretching. Those at 1029 and 760 cm^{-1} are the in-plane and out-of-plane C–H bends, respectively. The band at 1273 cm^{-1} is due to the phenolic C–O stretch.

The spectrum of adsorbed catechol was collected prior to any irradiation by 514 nm light. A constant, approximately equal in magnitude to the full height shown at 1357 cm^{-1}, was subtracted from the adsorbed-state spectrum in order to enhance the Raman peaks in the figure. The continuous background was probably fluorescence resulting from the formation of the charge-transfer complex. On adsorption, two bands

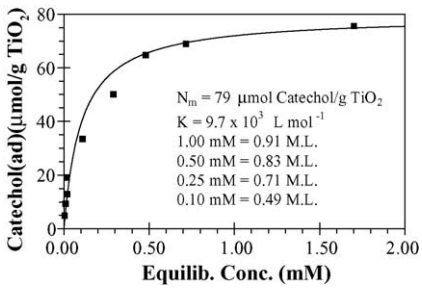

Fig. 2. Adsorption isotherm for initial monolayer of catechol on TiO_2 at 24 °C. The line is a fit to a Langmuir model.

present in the solution-phase spectrum were lost, those associated with in-plane and out-of-plane C-H bends (1029 and 760 cm^{-1}, respectively). Their absence suggests that those motions were restricted in the adsorbed state. The bands at 1357 and 1478 cm^{-1} were enhanced in the spectrum of catechol(ad) compared to catechol(aq.). Similar frequencies were reported by Connor et al. [7] in the infrared spectrum of catechol adsorbed to titanium dioxide—1333 and 1481 cm^{-1} in that study. (In fact, a weak peak occurs in the Raman spectrum at 1322 cm^{-1}, and may be diminished compared to the IR due to selection rules.) Connor et al. compared the IR spectrum of catechol/TiO_2 to those of catecholato complexes of Ti(IV) and found that the spectrum of $K_4[TiO(cat)_2]_2{\cdot}2H_2O$ complex was closest. Infrared peaks for that compound occurred at 1475 and 1247 cm^{-1}, which compared to 1258 and 1481 cm^{-1} in the FTIR spectrum of adsorbed catechol. On that basis, the bidentate (μ^2-oxo) structure was assigned to catechol(ad) [7].

Sanchez-Cortes et al. [10] studied adsorption of catechol on a metallic silver colloid and reported Raman spectra similar to the one in Fig. 3(b). In that study, the absence of CH bend frequencies in the spectrum of the adsorbed state was also noted, and the bands at 1329 and 1475 cm^{-1} were ascribed to polymer formation. However, the spectra of Sanchez-Cortes et al. had additional features not observed in this study. Sanchez-Cortes et al. reported a shift in the C=C stretching frequency to lower wavenumber, which was ascribed to increased conjugation of the ring on polymerisation. In this study, the C=C stretch shifted to higher wavenumber (1598 to 1611 cm^{-1}), consistent with decreased conjugation with the substituent oxygen atoms as a result of binding to oxophilic Ti(IV) ions. Sanchez-Cortes et al. also reported new resonances in the 200–500 cm^{-1} region, indicating a higher degree of ring substitution. In this study, no new peaks were observed in the low wavenumber region; only the TiO_2 peaks appeared there (445, 395, 196, and 141 cm^{-1}). It is reasonable to conclude, then, that very little, if any, polymerisation took place on the TiO_2 surface.

3.2. Persistence of the surface-bound photoproduct

When the 514-nm laser of the Raman microscope was focused onto the catechol/TiO_2 surface, a Raman spectrum with a high fluorescence background was observed. In air-saturated 1.0 mM solution, the fluorescence signal increases gradually with exposure time, reaching a plateau in about 60 min. The fluorescence signal was of primary interest in this study, as it was due to the product of a photoreaction. Raman signals could be better measured by switching to the 785-nm laser, which does not excite electronic states as efficiently as 514 nm.

The fluorescent photoproduct was surface-bound and persistent, as shown in Fig. 4. Fig. 4 is an image of the catechol/TiO_2 film after irradiation for 30 min with the 514-nm laser at high power (2.2 mW). The image was collected using an interference filter that passed a band of light 1600 ± 20 cm^{-1} from the 514 nm line. The spot is an image of the laser focus and its surrounding halo of scattered light. The fissures and other inhomogeneities evident in the image are due to the film.

The observation of a photochemical reaction implies that the surface complex, catechol/TiO_2, absorbs appreciably at 514 nm, although catechol and TiO_2 individually absorb only in the ultraviolet. The spectral shift on adsorption is well known; other authors [5,11,12] have reported a charge-transfer band for catechol/TiO_2 that spans much of the visible spectrum. In our adsorption experiments, we observed the development of a uniform yellow colour in the titania film, which deepened with catechol concentration. No colour change was observed in the solution phase.

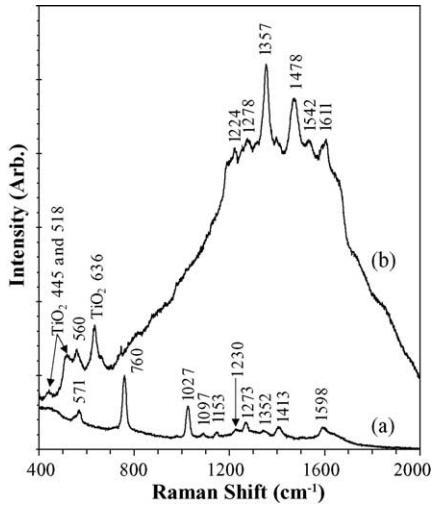

Fig. 3. Raman spectra collected with 785 nm laser of (a) 0.1 mol L^{-1} aqueous; and (b) TiO_2-adsorbed catechol.

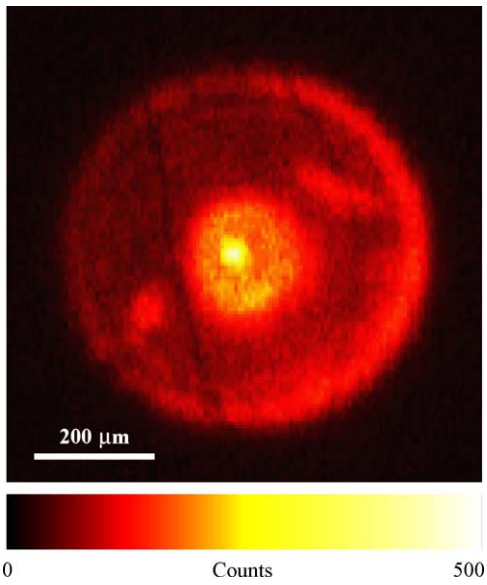

Fig. 4. Fluorescence image of catechol/TiO_2 film after 30 min laser exposure.

The present reaction is not a typical photo-oxidation reaction because the photo-generated holes are not the result of excitation from the valence band to the conduction band of titania. The band gap of anatase is much larger than the photon energy, 3.2 eV compared to 2.4 eV. Electronic excitation of the catechol/TiO_2 involves a HOMO-LUMO transition of the complex, followed by injection of the electron into the conduction band of TiO_2. The excited catechol complex carries a formal, positive charge, and can react. (Alternatively, the electron may be transferred back to the catechol, and the energy dissipated in radiative or non-radiative processes.) The reaction results in a product that is also able to absorb 514-nm light. Electronic excitation of the product can result in fluorescence to the ground state with even higher efficiency than the adsorbed catechol.

The long wavelength of excitation for this photoreaction is unusual. Fujihara et al. [2] mentioned an increase in TiO_2 fluorescence during photo-oxidation of isopropanol to acetone. Fluorescence development occurred on the same time scale as in this study, but the photon energy used was larger than the bandgap. The reaction kinetics were not studied.

3.3. Laser power dependence of the initial rate

Fig. 5 shows the laser power dependence of the reaction rate. The fluorescence signal was observed after irradiating the film with the beam attenuated by neutral density filters. The full laser power was 2.2 mW at the sample, and the film was irradiated at 1% (lower curve), 10% (middle curve), and 100% (top curve) of the full power. Four data sets are represented in p Fig. 5(a); although there is only one curve through the 10% power data, there are actually two replicate data sets (open and closed and triangles), which were generated from different films. The curves are shown to distinguish the data sets according to the laser powers used during the photochemistry phase. One point was removed from the 1% data set. The outlier lay far from the curve and was apparently the result of an instrumental problem that occurred during collection.

The time interval for the "photochemistry" phase of the experiment, during which the film was irradiated, was 2.00 min for 10% and 100% power, followed by 0.75 min for the measurement phase (1% power). For experiments in which the photochemistry phase was conducted at 1% power, the photochemistry interval was 1.25 min, followed by 0.75 min of measurement. The photochemistry interval was reduced for the experiments conducted at 1% power because it was recognised that photochemistry would occur during the probe phase as well as the photochemistry phase. By reducing the photochemistry interval to 1.25 min, the total time spent under the laser per cycle at the "photochemistry" power was 2.00 min, essentially the same as the 10% and 100% laser power experiments. (The correction term for the time under the "probe" laser is less significant at 10% and 100% laser power.)

The time axes of all the data sets in Fig. 5(a) have been corrected for irradiation of the surface during the measurement phase. Initial rates of reaction, estimated from the first few points of the data sets, were approximately proportional to the square root of the laser power (Rate $\propto$ Power$^{0.53}$). The square-root dependence is well known for oxidation reactions on titania [13]. The functional form indicates that (1) the reaction mechanism is first-order in the concentration of photo-generated holes and (2) the reaction occurs in the high power density regime, in which electron-hole recombination is significant. The observation of a square-root dependence also suggests that the reaction does not occur through a two-photon process, which might be possible at very high power densities. At double the frequency, the incident photons would have an energy of 4.8 eV, well above the band gap of TiO_2.

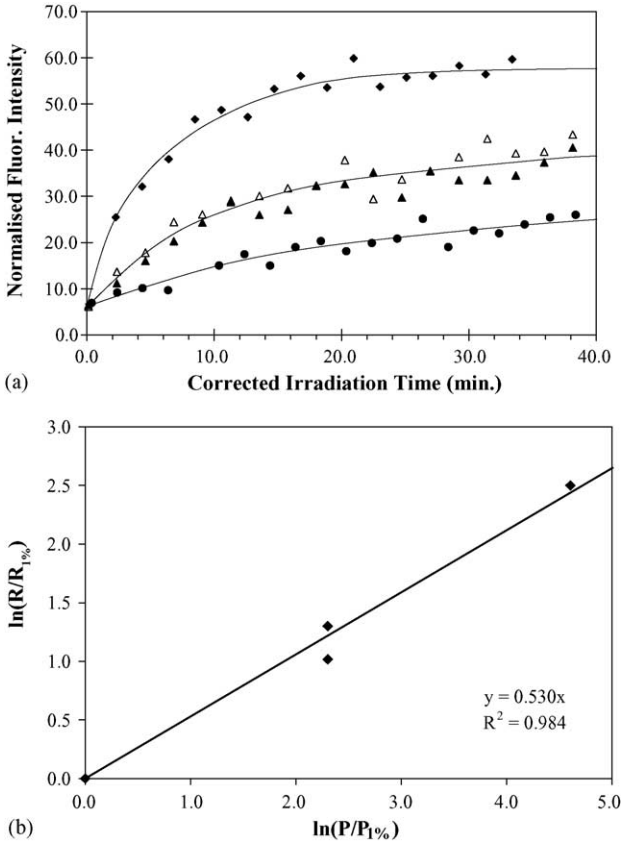

Fig. 5. Laser power dependence of reaction rate for air-saturated solution. (a) Time profiles of developing fluorescence (circles, 1% power; open and closed triangles, 10%; diamonds, 100%); (b) ln–ln plot of initial rates (relative to rate at 1% laser power) vs. laser power (relative to 1% laser power). The fit curve was forced through zero.

3.4. Oxygen dependence of fluorescence development

The formation of the fluorescent product was observed under three oxygen conditions: (1) nitrogen sparged solution; (2) air-saturated solution; and (3) oxygen-saturated solution.

Fig. 6 shows the kinetics of fluorescence production for four catechol coverages (θ = 0.49, 0.71, 0.83, and 0.91) under N_2-sparged solution. The solution was initially sparged for

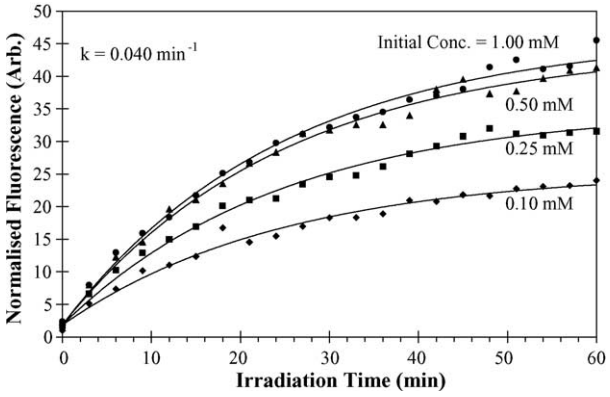

Fig. 6. Kinetics of fluorescence development under N_2-sparging. The lines are global fits to a first-order model with a single apparent rate constant ($k = 0.040\,\mathrm{min}^{-1}$).

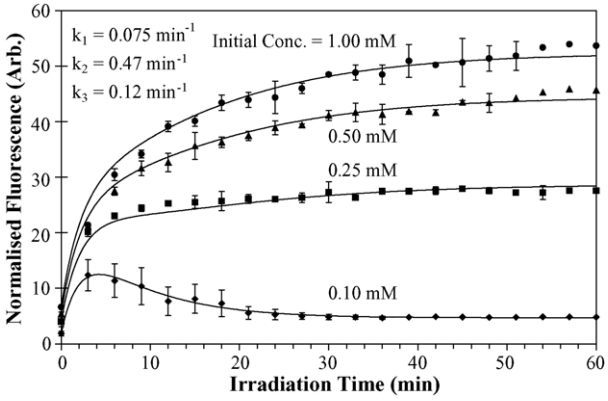

Fig. 7. Kinetics of fluorescence development under air-saturated solution. The lines are global fits to the model described in the text.

30 min prior to irradiation, in order to ensure that all oxygen was removed. Sparging continued as the reaction proceeded.

It is unusual for titania-catalysed oxidation reactions to proceed at all under a nitrogen-sparged solution. Catalytic photo-oxidation reactions involving TiO_2 require oxygen, or some other electron scavenger, to remove electrons from the surface. However, this reaction was not catalytic. Regeneration of the sites was not observed, and the steady-state reaction rate appeared to go to zero (or at least very small values) with time. The production of fluorescent centres was accompanied by depletion of the surface-adsorbed catechol, as confirmed by Raman experiments performed with a 785 nm probe laser (see next section).

Build-up of charge might be one reason why the reaction rate steadily decreased over time. However, the charge balance could have been maintained through electron scavenging by aqueous catechol. The one-electron reduction potential of catechol [14] is 530 mV (versus SHE at pH 7), and the equilibrium concentration of catechol in solution ranged from 0.10 to 1.00 mM (compared to ~0.3 mM for O_2 in air-saturated solution) so electron transfer from TiO_2 to catechol was possible. On the other hand, maintaining charge balance would not be a requirement for the reaction if the fluorescent product were a reduced Ti(III) ion. That could be achieved by removal of interstitial O^- by catechol as it reacted and desorbed.

The reaction kinetics could be fitted successfully with a first-order rate law:

$$I = I_\infty(1 - e^{-kt}) + b$$

where I is the fluorescence intensity of the product and I_∞ the maximum fluorescence signal. The background signal, b, was set to the average signal for all the data sets. All four data sets were fitted simultaneously using a simplex fitting routine. A single rate constant ($0.40\,\mathrm{min}^{-1}$) fitted all four data sets adequately when the maximum signal was allowed to vary. The initial rates determined from the fitting routine were in the same ratio as the initial coverages. Setting the relative value of the highest initial rate to 0.91 (to match the coverage), the relative initial rates were 0.48 ($\theta = 0.49$), 0.68 ($\theta = 0.71$), 0.87 ($\theta = 0.83$), and 0.91 ($\theta = 0.91$).

Fig. 7 shows the development of the fluorescence under air-saturated solution. The initial reaction rates increased dramatically in the presence of oxygen, as expected for photo-oxidation reactions on titanium dioxide. Oxygen is an electron scavenger, which depletes the concentration of photo-generated electrons in titania, reducing the probability of electron-hole recombination and increasing the lifetime of the holes. Consequently, the probability of the holes participating in a reaction is increased.

The kinetics under air-saturated conditions could not be fitted to a simple, first-order model, especially at lower coverage. For $\theta = 0.49$, the fluorescence signal rose to a maximum, and then decreased to a plateau. For $\theta = 0.71$, the transition from the initial rise in fluorescence to the plateau was too rapid to be first-order. The shapes of the kinetic data for the low coverages suggest that two pathways led to the product. One pathway produced a fluorescent product that later degraded to a non-fluorescent species (transient product), while the other pathway led to a persistent fluorescent species. The pathway to the transient product was oxygen dependent; it was not observed in the data for the nitrogen-sparged solutions.

The transient fluorescent species was more evident at the lowest coverage, and became less visible as coverage increased. The sharp transition to the plateau region of the $\theta = 0.71$ data suggests the same transient species contributed to the initial rise of the curve. At $\theta = 0.71$ and higher coverage the transient was obscured by the persistent species, which dominated at higher coverage. The change in the relative importance of the two pathways with coverage suggests that the transient pathway is associated with "defect" sites—e.g. steps and kinks—on the titania nanoparticles. Those sites have a higher free energy for adsorption, and so tend to fill earlier than the more co-ordinatively saturated sites (e.g. terrace sites). At lower coverages, catechol was bound primarily to the defect sites. At higher coverages, after all the defect sites were fully occupied, the catechol bound to the lower-energy

sites. Because defect sites have higher free energies, catechol adsorbed to them was more reactive. Therefore, reactions at defect sites went further—from adsorbed catechol, to a fluorescent species, to a non-fluorescent species (in the presence of O_2)—than reactions at non-defect sites, which were only able to undergo the first step to the fluorescent species, with or without O_2.

The reaction kinetics could be reproduced by a model like the one just described. In the model, catechol adsorbed to the sites with lower free energy (denoted C1) are able to react to form fluorescent centres (F1), but no further reaction is observed. First-order kinetics were assumed for simplicity.

$$\mathrm{C1(ad)} \xrightarrow[h\nu,O_2]{k_1} \mathrm{C1(ad)} \xrightarrow{\text{fast}} \mathrm{F1(ad)}$$

$$\frac{d\theta_{F1}}{dt} = k_1\theta_{C1} \quad (1)$$

where θ indicates surface coverage of the subscripted species. Eq. (1) integrates to

$$\theta_{F1} = \theta_{F1,\infty}(1 - e^{-k_1 t}) \quad (2)$$

where $\theta_{F1,\infty}$ is the coverage of F1 at the end of the reaction. Catechol adsorbed to sites with higher free energy (C2) react to form a fluorescent species (F2), which can react further to produce a non-fluorescent species (X).

$$\mathrm{C2(ad)} \xrightarrow[h\nu,O_2]{k_1} \mathrm{C2(ad)} \xrightarrow{\text{fast}} \mathrm{F2(ad)}$$

$$\mathrm{F2(ad)} \xrightarrow[h\nu,O_2]{k_3} \mathrm{X}$$

$$\frac{d\theta_{F2}}{dt} = k_2\theta_{C2} - k_3\theta_{F2} \quad (3)$$

$$-\frac{d\theta_{C2}}{dt} = k_3\theta_{C2} \quad (4)$$

Eqs. (3) and (4) are simultaneous rate laws. Eq. (4) is easily integrated to

$$\theta_{C2} = \theta_{C2,0}e^{-k_3 t} \quad (5)$$

and substituted into Eq. (3), which can then be solved as [15]

$$\theta_{F2} = \frac{k_2\theta_{C2,0}}{k_3 - k_2}(e^{-k_2 t} - e^{-k_3 t}) \quad (6)$$

The observed fluorescence signal is due to both F1 and F2:

$$S_F = a\theta_{F1} + b\theta_{F2} + c \quad (7)$$

The term, c, represents an observed fluorescence background that develops prior to irradiation. (As already noted, the catechol/TiO_2 fluoresced modestly as soon as it adsorbed. The fluorescence development described by the model is light-dependent, as illustrated by Figs. 4 and 5.) Factors a and b represent the relative intensities of F1 and F2.

The lines through the data represent fits to the model described. The fitting was performed on all curves simultaneously, to obtain global values of k_1, k_2, and k_3. The background (c) values were set to the initial value of each of the data sets and were not varied. The fit assumed that the amount of C2 (catechol adsorbed to defect sites) was constant for all coverages; i.e., the defect sites were saturated by $\theta = 0.49$. Considering its simplicity, the model reproduced the observed data adequately, although some systematic error is evident in the 0.50 mM ($\theta = 0.71$) and 1.00 mM ($\theta = 0.91$) data.

A number of subtleties are not accounted for in the model. The model specifies two types of surface adsorption site—defects and co-ordinatively saturated sites (e.g. terrace sites)—at which the photochemical reactions are presumed to take place. In fact, a number of possible defect sites (e.g. steps, kinks, vacancies) would be expected, all of which would have different energies. There should also be a number of different terrace sites, owing to the range of different surfaces exposed on the nanoparticle. Therefore, ascribing only a single rate constant, k_1, to the production of the persistent products is most likely an over simplification. The same could be said for k_2 and the production of transient products. Within the two classes of fluorescent product (transient and persistent) there should also be a range of energies owing to the different adsorption sites from which they arise, so employing a single rate constant, k_3, is also too simple. It may even be possible for higher O_2 concentrations to drive the destruction of some of the higher energy "persistent" products. Generation of a broad range of products from many different adsorption sites is consistent with the broad fluorescence observed. While the model suffers somewhat from its simplicity, it does reproduce the essential features of the kinetics with a single set of k_1, k_2, and k_3 for all the catechol coverages under air saturated conditions.

The rate constant k_1 was approximately double that of the first-order rate constant obtained in nitrogen-sparged solution (0.075 min^{-1} compared to 0.040 min^{-1} for anoxic conditions), suggesting that the oxygen acts as an electron scavenger for this reaction. The rate constant, k_2, of fluorescence production from C2 was much higher at 0.47 min^{-1}, while k_3, for destruction of the transient fluorescent species, F2, was 0.12 min^{-1}. The relatively high rate constant for C2 compared to C1 is consistent with the expectation of higher reactivity for catechol adsorbed to defect sites.

When the solutions were saturated with O_2, the initial rates increased again (Fig. 8), confirming the role of O_2 as an electron scavenger in the production of the fluorescent product. Under oxygen-saturated conditions, the transient became more evident at the higher catechol concentrations. That is probably because the apparent rate constants for production and depletion of the transient product increased with oxygen concentration, so that the transient became narrower and higher. It is also possible some of the adsorbed catechol molecules that were not reactive under air saturation were able to react under oxygen-saturated conditions. The lower

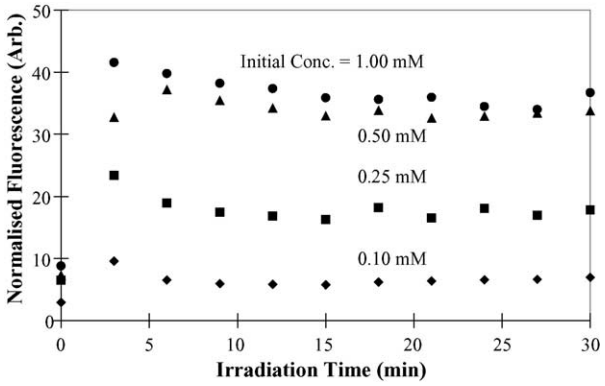

Fig. 8. Fluorescence development under O_2-saturated solution.

normalised fluorescence signals observed under oxygen saturation suggest that was the case. The previously described model was not used to fit the data for oxygen-saturated conditions because only the tail of the transient was observed under oxygen saturation. The early part of the reaction was too fast to observe with the Raman microscope, and so the amplitude of the transient could not be estimated reliably.

3.5. Raman microprobe of the irradiated area with 785 nm light

The irradiated surface could be probed for adsorbed catechol and organic products during the reaction by switching lasers from 514 nm (used for stimulating the photoreaction and for probing the fluorescence development) to 785 nm. The longer wavelength is less effective for stimulating electronic excited states, so the relatively small Raman signals were not obscured by the counting noise of the fluorescence background signal. However, the spot size of the 785 nm laser was greater than that of the 514 nm laser, so some of the (nominally) non-irradiated surface was also probed in those measurements.

Fig. 9 shows a series of Raman spectra of the catechol/TiO_2 surface, collected after irradiation at 514 nm for 0–30 min. The spectra were normalised to the TiO_2 peaks. Catechol Raman intensities (560 cm^{-1} and 1100–1700 cm^{-1}) all decrease with irradiation time. No new Raman signals appear, even in the low-wavenumber region (200–500 cm^{-1}) as expected for multiply substituted rings. The absence of new features in the spectra suggests that the decay of catechol Raman signals is due to desorption. The adsorbed catechol was probably partially oxidised at the surface following the initial charge transfer. The enthalpy change on oxidation would produce a local heating effect, resulting in desorption. We have observed, by infrared spectroscopy, similar behaviour for other small molecules (e.g. phthalate, salicylate) adsorbed on titania, when irradiated with UV light.

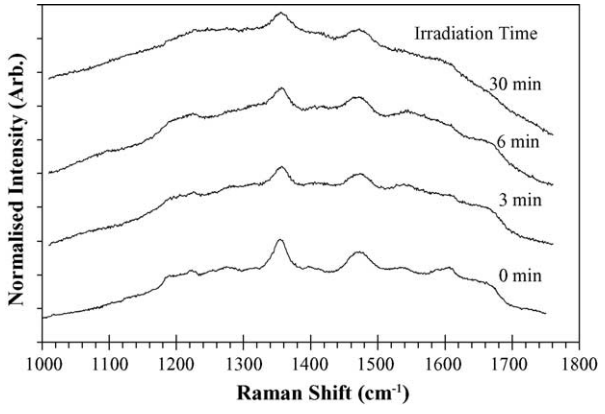

Fig. 9. Depletion of surface-adsorbed catechol in air-saturated solution during irradiation at 514 nm. The Raman traces were collected using a 785 nm laser.

Desorption (and presumably oxidation) of catechol was accompanied by an increase in fluorescence. Because the spectrum showed no changes in the Raman spectrum of catechol, the fluorescence was probably caused by a modification of the titanium dioxide surface that occurred during the oxidation and desorption of catechol. That scenario is consistent with the previously described kinetic model. The reaction rates at the two classes of surface site would depend on their free energies and the degree of unsaturation, as would the susceptibility of the products (modified surface sites) to attack by dissolved oxygen. The fact that dissolved oxygen is capable of destroying the fluorescent centres implies that the fluorescence was due to Ti(III) ions produced during electron transfer from adsorbed catechol. Dissolved oxygen can re-oxidise the Ti(III) ions back to Ti(IV) with the energy supplied by the laser. Sekiya et al. have also implicated partially reduced titanium ions in the luminescence of their anatase films [4].

4. Conclusions

The fluorescence of a catechol/TiO_2 (nanocrystal) film increased as the film was irradiated with 514 nm light. The reaction was a single-photon process, as evidenced by the square-root power dependence of the initial rate, and was not catalytic. The presence of dissolved oxygen had a positive effect on the initial rate of reaction. A further photochemical reaction in the presence of dissolved oxygen resulted in the permanent removal of some of the fluorescent sites. The likely explanation is that two classes of adsorption site were available on the surface. High-energy sites, such as steps and kinks, resulted in high-energy products that could further react in the presence of oxygen and green light. Low-energy sites, such as terraces, led to lower energy products that could not react further. Raman spectra collected with a 785 nm laser suggested that the fluorescent product was a partially reduced titanium ion.

Acknowledgments

The authors wish to acknowledge the assistance of R.S. Wylie (Ryerson) for providing the fitting routine. Funding

for this research was provided by a Discovery Grant from the Natural Sciences and Engineering Research Council of Canada. The Raman microscope was funded by the Canada Foundation for Innovation, the Ontario Innovations Trust, and Ryerson University.

References

[1] A. Suisalu, J. Aarik, H. Mänder, I. Sildos, Thin Solid Films 336 (1998) 295–298.
[2] K. Fujihara, S. Izumi, T. Ohno, M. Matsumura, J. Photochem. Photobiol. A: Chem. 132 (2000) 99–104.
[3] R. Janes, M. Edge, J. Rigby, D. Mourelatou, N.S. Allen, Dyes Pigments 48 (2001) 29–34.
[4] T. Sekiya, S. Kamei, S. Kurita, J. Lumines. 8789 (2000) 1140–1142.
[5] J. Moser, S. Punchinhewa, P.P. Infelta, M. Grätzel, Langmuir 7 (1991) 3012–3018.
[6] S.A. Haque, Y. Tachibana, R.L. Willis, J.E. Moser, M. Grätzel, D.R. Klug, J. Durrant, J. Phys. Chem. B 104 (2000) 538–547.
[7] P.A. Connor, K.D. Dobson, A.J. McQuillan, Langmuir 11 (1995) 4193–4195.
[8] S. Pivovarov, J. Colloid Interf. Sci. 196 (1997) 321–323.
[9] G. Socrates, Infrared and Raman Characteristic Group Frequencies: Tables and Charts, Wiley, Chichester/Toronto, 2000, pp. 157–165.
[10] S. Sanchez-Cortes, O. Francioso, J.V. Garcia-Ramos, C. Ciavatta, C. Gessa, Colloids Surf. A: Physicochem. Eng. Aspects 176 (2001) 177–184.
[11] R. Rodriguez, M.A. Blesa, A.E. Regazzoni, J. Colloid Interf. Sci. 177 (1996) 122–131.
[12] Y. Liu, J.I. Dadap, D. Zimdars, K.B. Eisenthal, J. Phys. Chem. B 103 (1999) 2480–2486.
[13] C.S. Turchi, Proceedings of a Workshop on Potential Applications of Concentrated Solar Energy, National Research Council, National Academic Press, 1991, pp. 16–18.
[14] S. Steenken, P. Neta, J. Phys. Chem. 83 (9) (1979) 1134–1137, http://www.rcdc.nd.edu/compilations/Red/RED_501.HTM, online reproduction of Peter Wardman, J. Phys. Chem. Ref. Data 18(4) (1989), 1637–1755.
[15] R.G. Mortimer, Physical Chemistry, 2nd ed., Academic Press, Toronto, 2000, pp. 420–422.